

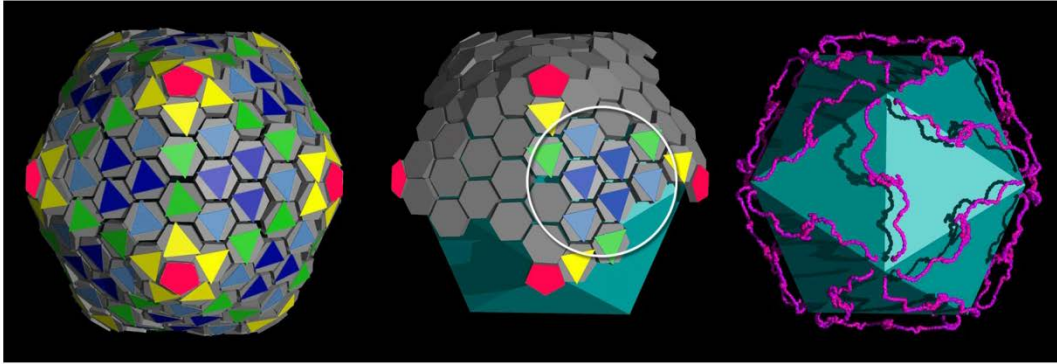
Electronic Supplementary Information

Membrane-containing virus particle exhibits mechanics of a composite material for genome protection

S. Azinas,^{a,b} F. Bano,^b I. Torca,^c D. H. Bamford,^d G. A. Schwartz,^e J. Esnaola,^c H. M. Oksanen,^d
R.P. Richter,^{b,f,*} N.G. Abrescia,^{a,g,*}

-
- a. Molecular recognition and host-pathogen interactions programme, CIC bioGUNE, CIBERehd, Derio, Spain.*
- b. Biosurfaces Lab, CIC biomaGUNE, San Sebastian, Spain.*
- c. Mechanical and Industrial Production Department, Mondragon University, Arrasate- Mondragón, Spain.*
- d. Molecular and Integrative Biosciences Research Programme, Faculty of Biological and Environmental Sciences, Viikki Biocenter, University of Helsinki, Finland.*
- e. Centro de Física de Materiales, (CSIC-UPV/EHU) & Donostia International Physics Center, San Sebastian, Spain.*
- f. School of Biomedical Sciences, Faculty of Biological Sciences, School of Physics and Astronomy, Faculty of Mathematics and Physical Sciences, and Astbury Centre for Structural Molecular Biology, University of Leeds, Leeds, United Kingdom. Email: R.Richter@leeds.ac.uk; TEL: +44 113 3431969*
- g. IKERBASQUE, Basque Foundation for Science, Bilbao, Spain. Email: nabrescia@cicbioqune.es; FAX: +34 946572502; TEL: +34 946572523*

a



b

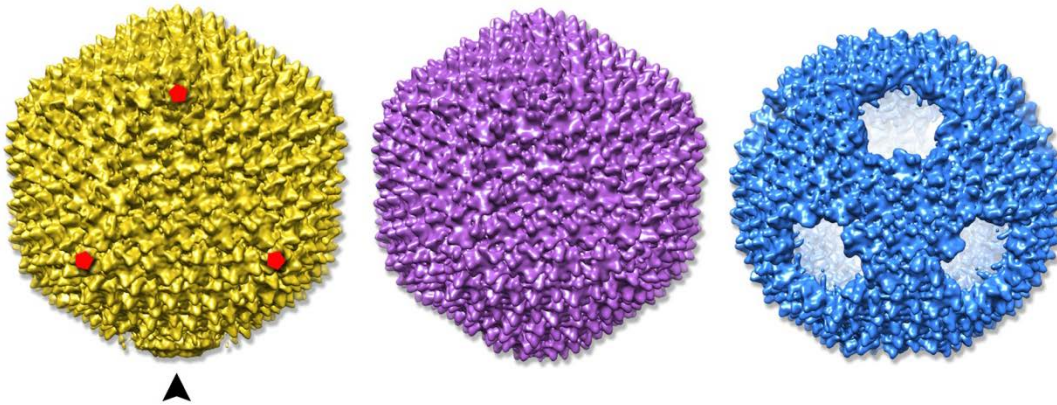


Fig. S1. (a) Left: schematic representation of PRD1 where the P3 major capsid protein with a double β -barrel fold forms trimers (colored triangles) with the morphological appearance of pseudo-hexagons (grey). The yellow (peripentonal), green, light-blue and blue triangles indicate the independent capsomers within the icosahedral asymmetric unit; red corresponds to the penton protein composed of P31 protein. P31 is part of the spike complex that also contains membrane protein P16, spike protein P5, and receptor binding protein P2 (not shown). Centre: as in left, but with lower capsomers removed to reveal the underlying membrane vesicle (cyan). The white circle marks capsomers forming the group of nine (GON; green, light-blue, and blue triangles) that constitutes the central part of a virus facet. Right: schematic PRD1 with all capsomers removed to show the presence of the cementing protein P30 (magenta) running along the facets of the virus; (b) Left: cryo-EM map (C1 symmetry) of PRD1 (EMDB: 5984) at 12 Å resolution (contoured at 0.5 threshold-level in Chimera⁴⁵) showing the spiky appearance of the particle due to the β -barrels of the P3 major capsid proteins. Red pentagons mark the five-fold vertices of a triangular virus facet and the black arrow-head indicates the unique vertex. Centre: cryo-EM map of Sus1 procapsid at 14 Å resolution (EMDB: 1013), contoured at 2.3 threshold-level. A unique vertex is not visible because the map is 60-fold averaged. Right: cryo-EM icosahedral map of P3-shell particle at 12 Å resolution (EMDB: 1014) contoured at 3.0 threshold-level.

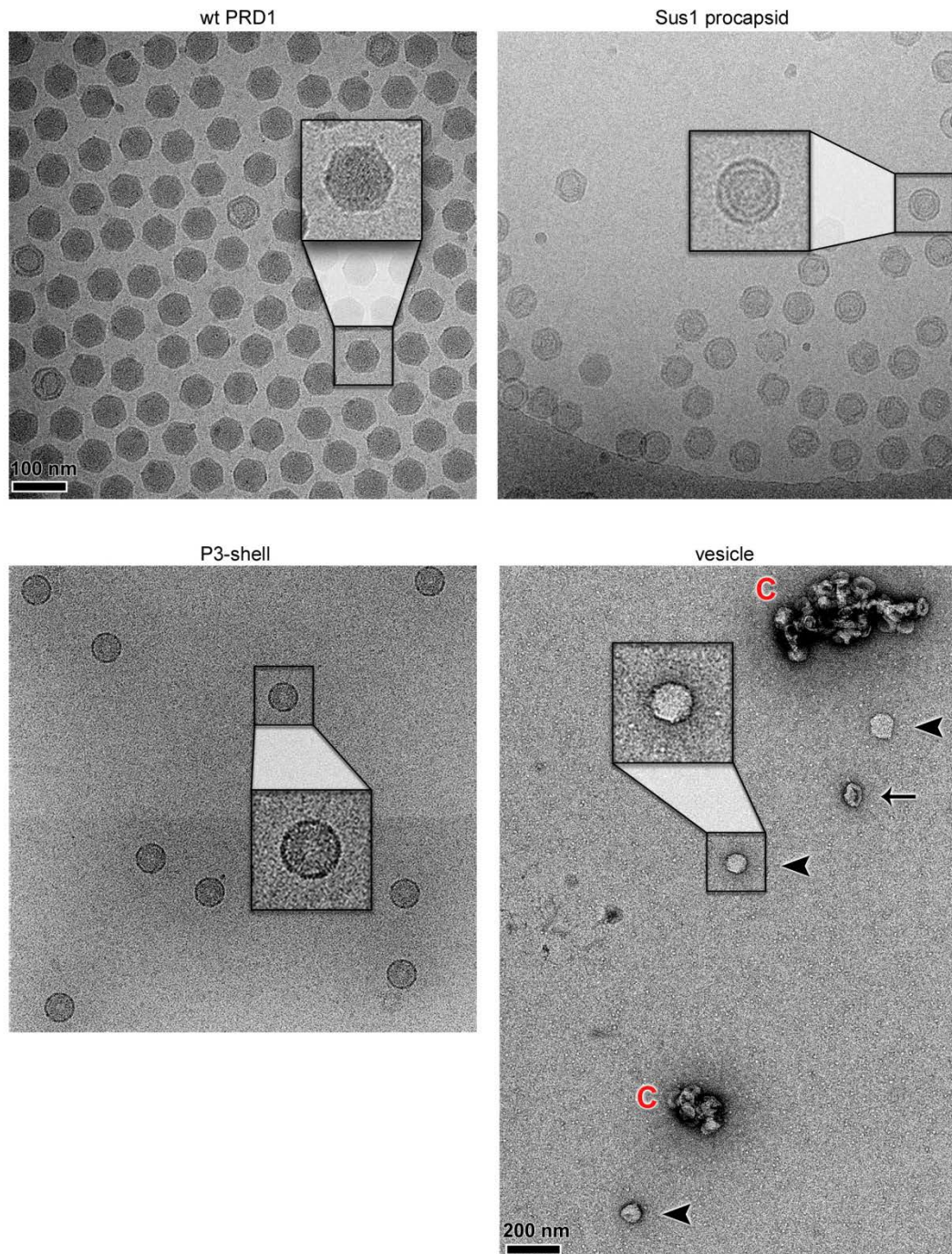


Fig. S2. Cryo-EM images of aged samples (2 to 4 weeks) of wt PRD1, Sus1 procapsid and P3-shell particles (all to scale to the scale-bar in wt PRD1); proteo-lipidic vesicles were imaged by negative-stain EM due to the lower abundance of particles resulting from a more stringent purification protocol (see Experimental). Corresponding insets are 2× magnified. In the case of wt PRD1 more than 96% of the particles are intact and exhibit a homogeneous dark interior, whereas in DNA-devoid particles the interior is lighter and the internal membrane is apparent as a thin ring inside the icosahedral proteinaceous shell. This morphology is clearly displayed by

the DNA-packaging defective Sus1 procapsid. The P3-shell particles lack the membrane and the proteinaceous shell is more spherical due to the lack of penton proteins (P31) and the peripentonal MCPs P3 (see Fig. S1b, right) which stabilize the facets of the icosahedron. In the vesicle negative-stain image black arrowheads indicate DNA-full vesicles whereas the black arrow points at a deformed vesicle and the red letter 'C' to clumps of vesicles deformed and likely to have lost or in the process of losing the viral genome.

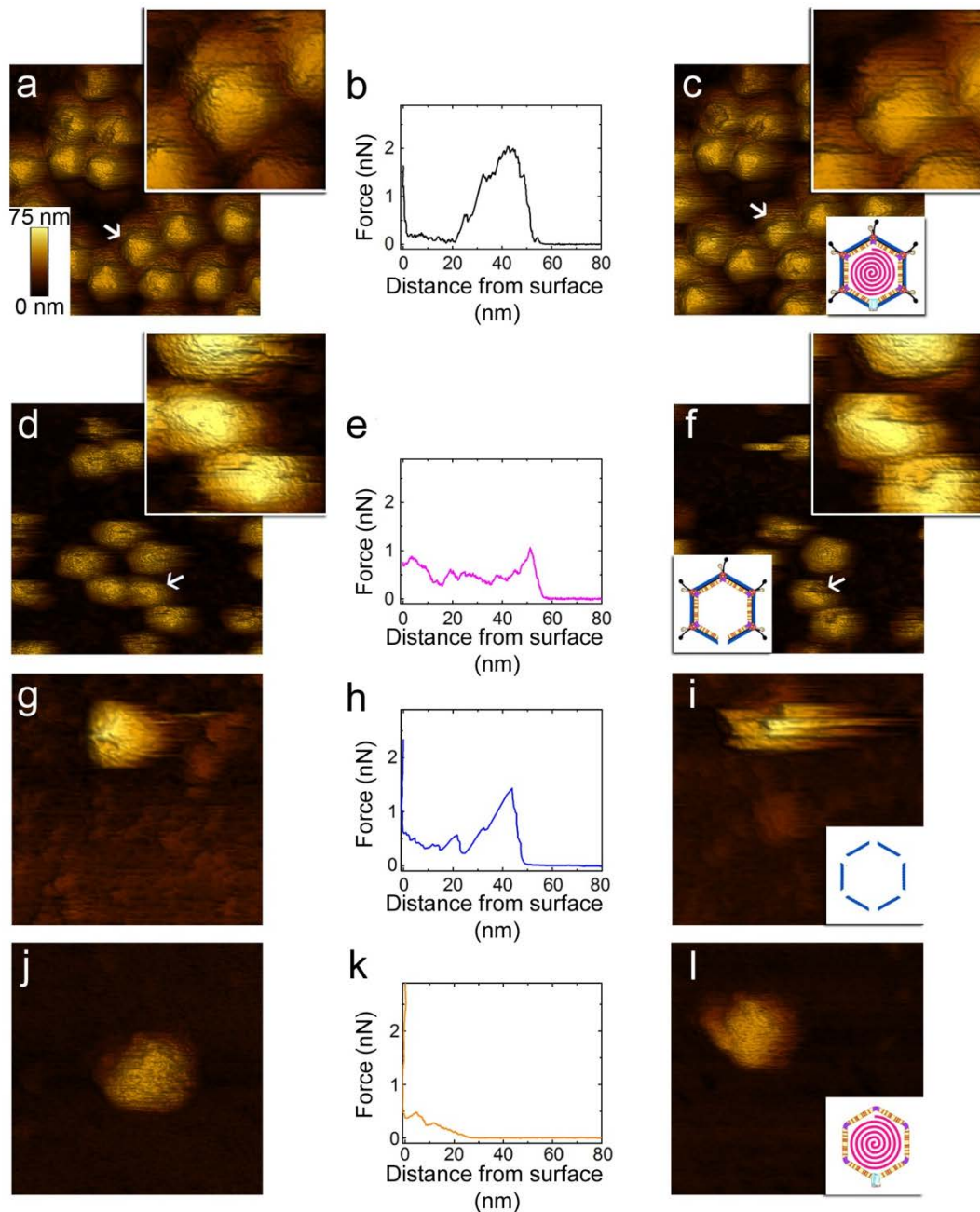


Fig. S3. Consecutive images of PRD1 particles before (a), (d), (g) and (j) and after (c), (f), (i) and (l) nanoindentation; schematics identify the corresponding particle types, from top to bottom: wt PRD1, Sus1 procapsid, P3-shell, and vesicle. (b), (e), (h) and (k) represent a single mechanical indentation, with the corresponding force curve obtained for each particle type. Image size: 500 nm; z range: 75 nm (see color key in a). The indented particle is marked with an arrow in a, c, d, and f; insets show enlarged images (image size: 160 nm) of the indented particle - from (a) and (c) insets at least twelve capsomeres appear to be displaced. Upon acquisition of the force curve shown in e, the z travel was set slightly too short to capture the hard wall contact (see Experimental for details). The indicated distance, therefore, should be considered as being marginally smaller than the real distance from the surface.

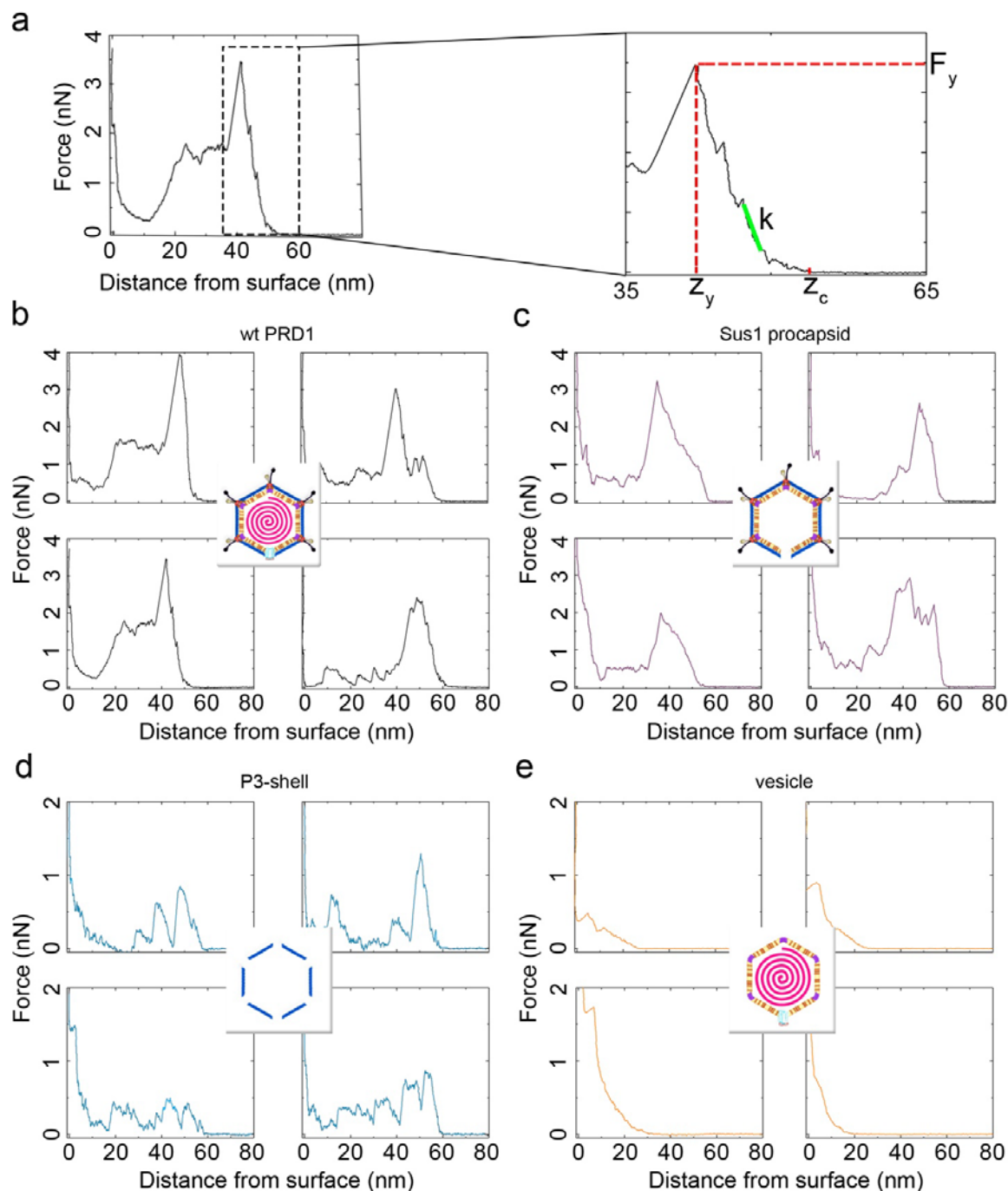


Fig. S4. (a) Sample force curve with extracted parameters indicated: yield force, F_y , stiffness, k (equivalent to the negative slope of the linear fit in green), and yield strain, $\varepsilon_y = (z_c - z_y) / h$, where h is the particle height (Fig. 2, left panel). All parameters were measured directly from the force curves and used to compile the histograms in Fig. 2 (other panels); (b)-(e) Four representative force curves for each of the four PRD1-derived particle types that were selected for further analysis. The variability in the shape of the force curves for each particle type may be due to variations in the particle orientation on the surface, the exact position of the indenting AFM tip on the particle, and possibly also stochastic variations in the yield behavior.

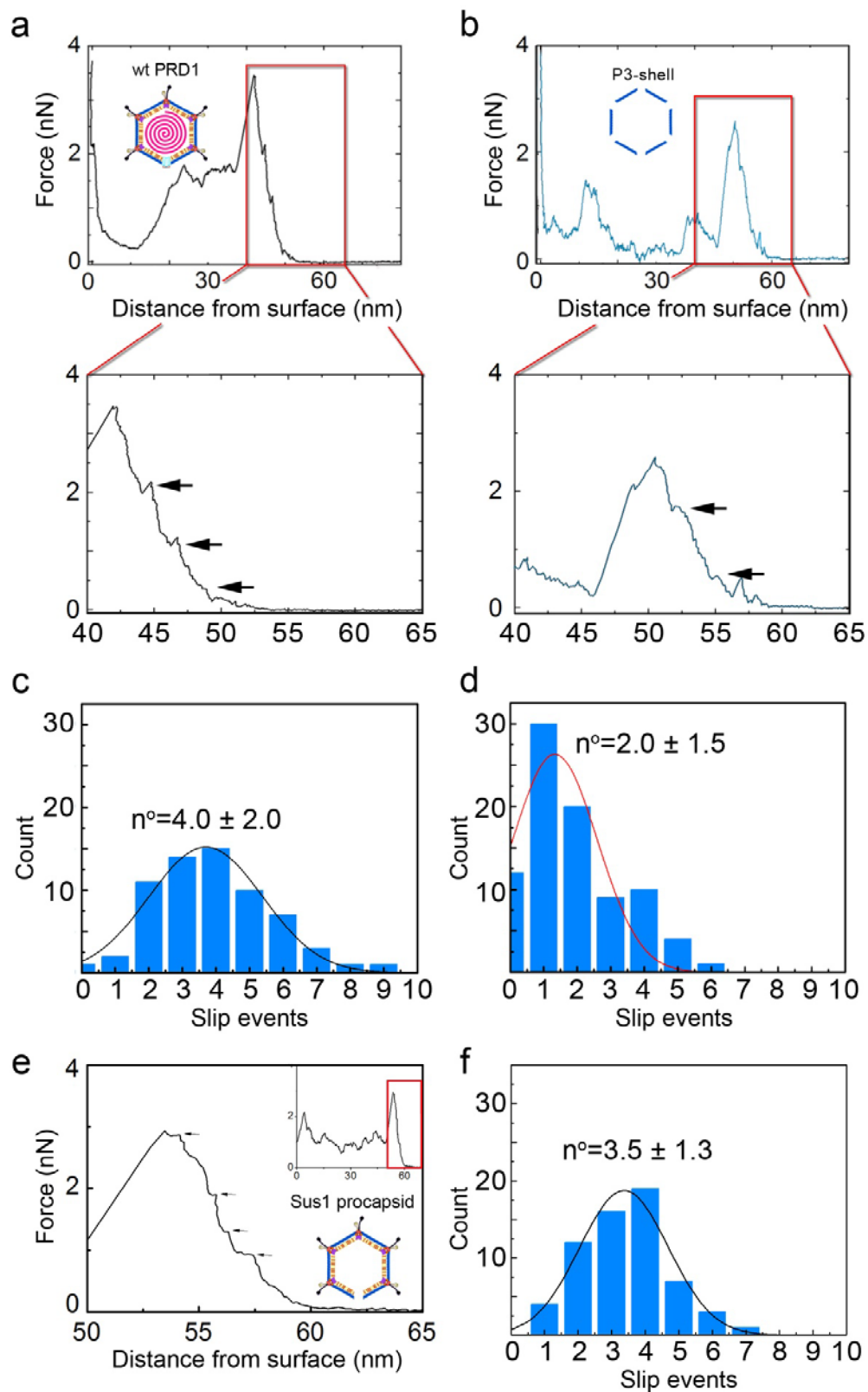


Fig. S5. Analysis of slip events (microfractures). Representative force vs. distance curve of wt PRD1 (a) and P3-shell (b); insets highlight stochastic slip events during loading (black arrows

indicate micro-fractures). We defined a slip event as a 0.4 nm to 1.5 nm decrease in probe-sample distance that is associated with a decreasing or constant force and occurs before the particle yields. Smaller distances were discarded to avoid noise interference and larger distances were classified as yield. Histograms with Gaussian fit (mean \pm s.d.) of the number of slip events (n^o) before yielding for (c) wt PRD1 and (d) P3-shells. (e), (f) equivalent data for the Sus1 procapsid. Comparison of the mean values with the yield forces for wt PRD1 (3.0 nN), Sus1 procapsid (2.7 nN) and P3-shell (0.9 nN; Fig. 3a) reveals similar micro-fracture rates of 1.3, 1.3 and 1.4 per nN of applied force, respectively.

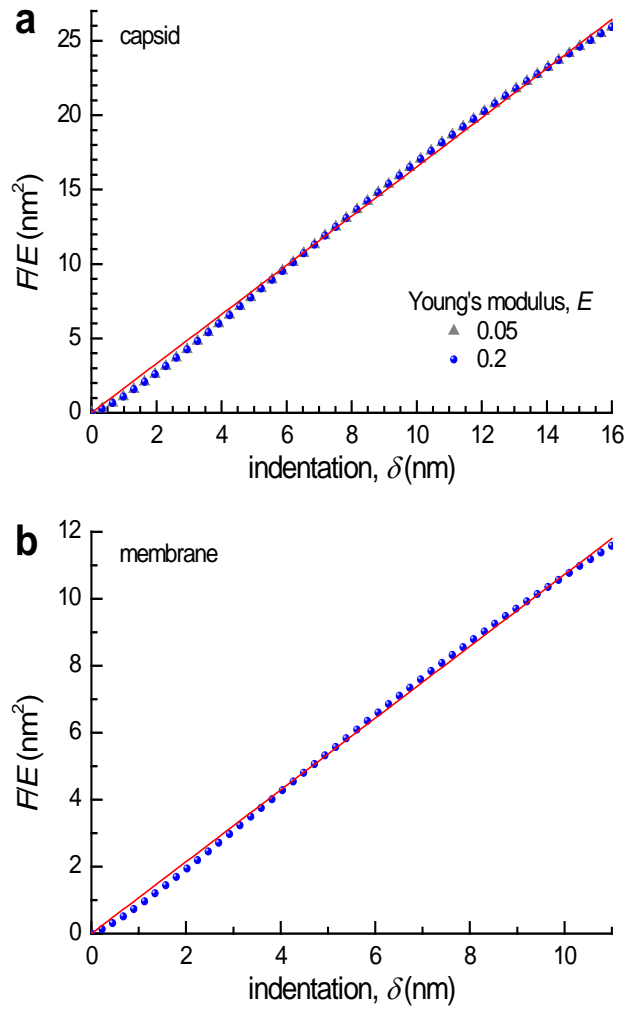


Fig. S6. Simulations with finite-element analysis. (a) Elastic shell (capsid): force scaled with Young's modulus F/E vs. indentation δ for a single spherical shell with a size representing the PRD1 capsid (outer radius $R = 33.2$ nm, thickness $d = 8$ nm). Data for $E = 0.05$ GPa and 0.2 GPa are shown (grey triangles and blue dots, respectively); these overlap fully, demonstrating that the Young's modulus is a simple scaling parameter and does not affect the curve shape. The red line is a linear fit through the origin (slope $\alpha = 1.65$ nm); (b) Elastic shell (membrane): F/E vs. δ for a single spherical shell with a size representing the membrane ($R = 25.2$ nm, thickness $d = 5.5$ nm). The red line is a linear fit through the origin (slope $\alpha = 1.07$ nm). All data shown here were computed with a Poisson ratio of 0.4; see Fig. S7 for an analysis of the effect of the Poisson ratios on the outcome of the modelling.

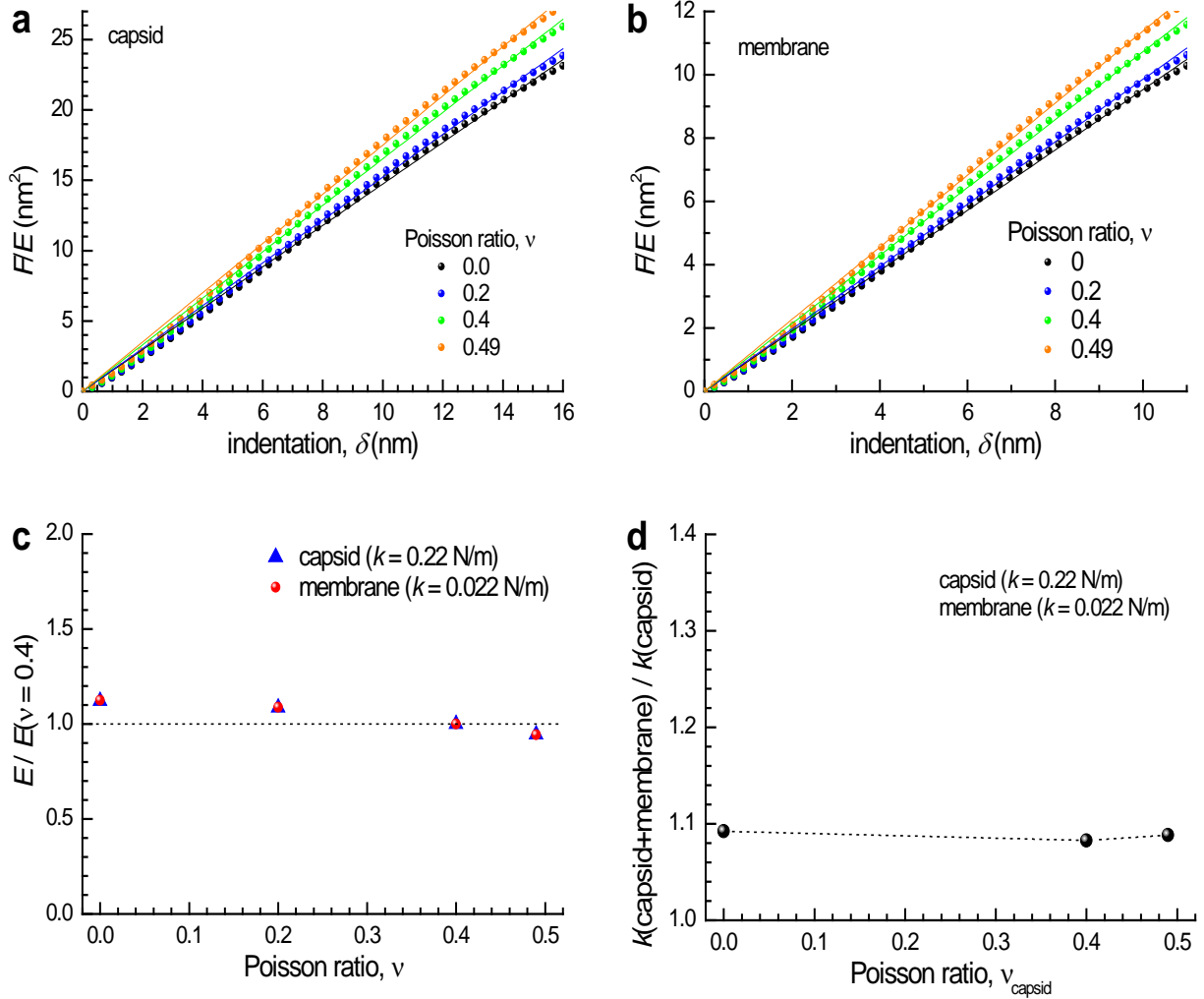


Fig. S7. Test of sensitivity to Poisson ratios. All data shown are from simulations with finite-element analysis, analogous to Fig. 5. (a)-(b), Force scaled with Young's modulus F/E vs. indentation δ for single elastic spherical shells with a size representing the PRD1 capsid (outer radius $R = 33.2$ nm, thickness $d = 8$ nm; (a)), and the membrane ($R = 25.2$ nm, thickness $d = 5.5$ nm; (b)). Data for selected Poisson ratios ν ranging between 0 and 0.49 (as indicated in the panels) are shown as symbols. The lines in matching colors are linear fits through the origin, and reproduce the data equally well for all ν . (c) Young's modulus E vs. Poisson ratio ν for a capsid with stiffness $k = 0.22$ N/m and a membrane with stiffness $k = 0.022$ N/m (i.e. values close to those observed experimentally for the P3-shell and the vesicle, respectively, cf. Fig. 3). E is normalized by the Young's modulus value obtained at a Poisson ratio $\nu = 0.4$, and the data show that variations relative to this reference are generally small (from -6% to 12%). (d) Enhancement in stiffness k predicted for the capsid-membrane composite compared to the capsid alone as a function of the capsid's Poisson ratio. The relative enhancement is virtually independent of the capsid's Poisson ratio. The membrane's Poisson ratio did not affect k of the capsid-membrane composite appreciably (not shown).

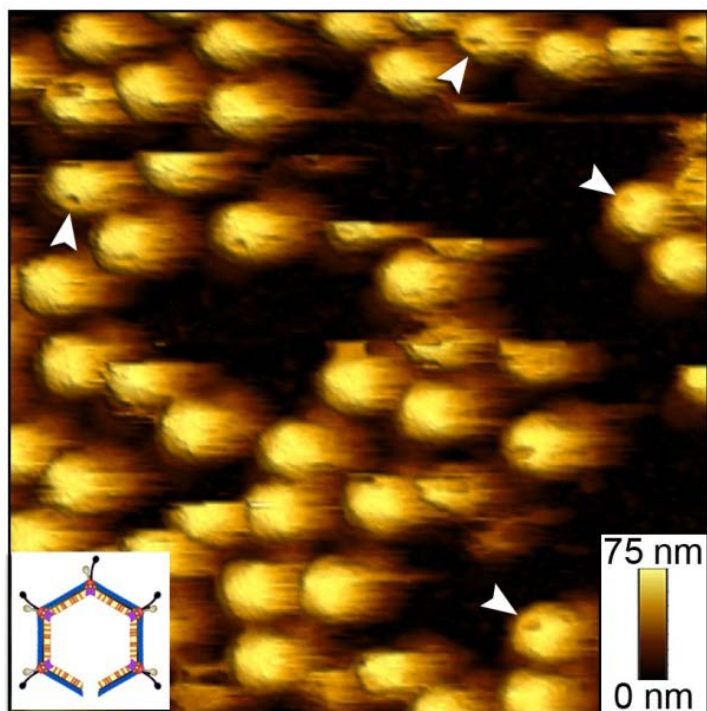











Fig. S8. Representative image at lower resolution covering a large set of Sus1 procapsids used for the statistical analysis; white arrow-heads mark the location of the unique vertex of the differently oriented procapsids. Some particles were displaced upon imaging and are therefore only partially visible. Image size: 1 μm ; z range: 75 nm (see color key).

Table S1. Identification of protein P30 in the PRD1 P3-shell by mass spectrometry

PDB Acc. No.	Number of unique peptides	Unique peptides	Modifications	Coverage ^a	Identification
1W8X M	4	AVAEQTYHAIGTGIQmGQTFNQPLINTQEG QFmPFLQGPHR QFMPFLQGPHR VEGRIAGIQQAR IAGIQQAR	M16, oxidation M3, oxidation	63.9 %	<i>Tectiviridae</i> family, minor capsid protein P30 of bacteriophage PRD1

^a Percentage of the protein sequence covered by identified peptides

Table S2. Mechanical properties for PRD1 particles from this study and values for other dsDNA viruses taken from the literature. Symbols and colors on the left are described in the key legend in Fig. 5.

	Virus	h (nm)	k (N/m)	F_y (nN)	ϵ_y (%)	T (10^5 J/m ³)	E (GPa)	Reference
	PRD1	67.6	0.57	3.0	17.5	2.2	--	This study
	Sus1 procapsid	66.9	0.39	2.7	18.1	2.1	0.24	This study
	P3-shell	62.8	0.22	0.9	12.3	0.54	0.13	This study
	HSV-1	125	0.52	5.8	16.0	1.1	1.0	37, 38, S1
	Bacteriophage P22 capsid	50	0.19	1.1	12.0	1.0	0.2	2
	Bacteriophage λ	63	0.25	1.6	12.7	1.0	1.0	36
	Adenovirus	95	0.46	3.3	31.6	2.2	--	41
	Bacteriophage T7	60	0.17	0.82	16.2	0.7	--	S2
	Bacteriophage HK97	54	0.11	0.9	15.7	0.9	0.6	S3

h , particle height (measured by AFM; see Fig. 2 for PRD1 data)

k , stiffness

F_y , yield force

$\epsilon_y = (z_c - z_y) / h$, yield strain

$T = (6 F_y \epsilon_y) / (\pi h^2)$, toughness

E , capsid Young's modulus

SUPPLEMENTARY REFERENCES

- S1. I. Liashkovich, W Hafezi, J. E. Kühn, H. Oberleithner, A. Kramer, V. Shahin, *J. Cell. Sci.*, 2008, **121**, 2287-2292.
- S2. M. Hernando-Perez, E. Pascual, M. Aznar, A. Ionel, J. R. Castón, A. Luque, J. L. Carrascosa, *Nanoscale*, 2014, **6**, 2702-2709.
- S3. W. H. Roos, I. Gertsman, E. R. May, C. L. Brooks, J. E. Johnson, G. J. Wuite, *Proc. Nat. Acad. Sci. U. S. A.*, 2012, **109**, 2342-2347.